© JUN 2025 | IRE Journals | Volume 8 Issue 12 | ISSN: 2456-8880

Cross-Diffusion Analysis of Heat and Mass Transfer Effects of Unsteady Mhd Viscoelastic Flow Over Exponentially-Stretching Vertical and Inclined Porous Media

MFEBE, J. F.[1], AMOO, S. A.[2], ANYANWU, E. O[3]
[1, 2, 3]*Department of Mathematics, Federal University Wukari, Nigeria*

Abstract- The development of a mathematical model for the 2D unsteady MHD viscoelastic flow over exponentially-stretching vertical and inclined porous media is the primary aim of this research. The combined effects of Soret and Dufour, activation energy, viscous dissipation, thermal radiation, mixed convection, thermal heating are included in the energy and concentration equations within this model. By using appropriate similarity transformations, the governing partial differential equations (PDEs) were transformed into nonlinear ordinary differential equations (ODEs) and then solved numerically using the embedded classical Runge-Kutta method along with the shooting techniques. The impact of various physical parameters on concentration, velocity, and temperature profiles were shown through graphs. It was found that increase in heat source (γ) and thermal conductivity (σ) decreases the heat transfer rate but increases the skin friction and mass transfer rates. It was further discovered that the increase in thermal Grashof (Gr) and solutal Grashof (Gc) increases skin friction, heat and mass transfer rates, whereas the reverse trend was noticed for the magnetic strength. The temperature diminishes as the Prandtl number increases, whereas the opposite scenario exists for Dufour and radiation. The fluid concentration rises for a monotonic increment of the Soret, while it reduces for Schmidt number and chemical reaction. The amplification of skin friction is observed with an increase in magnetic field strength, while it decreases with an increasing viscoelastic ratio factor. The Nusselt number decreases as radiation increases but the opposite scenario occurs with increases in the Prandtl number. The Sherwood number is heightened by an increase in the Schmidt number, reaction. Moreover, the numerical values of skin friction and the Nusselt number are compared with the previously published work, demonstrating excellent agreement between the results.

I. INTRODUCTION

MHD fluid flow is essential in engineering and industrial processes and can be translated into mathematical models. To forecast the behavior and distinctiveness of heat and mass transfer of such fluids accurately, it becomes essential to study the velocity profiles, temperature parameters and concentration behavior of the flow, hence the rate of heat absorption or generation of such a system with chemical reactions. Also, the study of fluid flow through Darcy permeable media with radiation, Dufour and Soret effects were incorporated (Amoo and Idowu, 2018). The heat energy transfer and boundary layer fluid flow on a stretching and/or shrinking surfaces are the topics of intensive investigations since the basic work performed by Crane (1970), because of its immense technological applications. Some of them are; electronic chips and metallic sheets cooling, preparation of plastic sheets, crystal growth, paper production, materials manufacturing and so forth (Moradikazerouni *et al*, 2019, Moradikazerouni, (2019). Some important aspects of flowing fluid on stretching surface are addressed by Andersson *et al.* (2018), and Vajravelu (2001). Cross diffusion is normally the combined effect of the mass and thermal diffusion. The transport analysis is mainly concerned with Soret and Dufour effects. These two effects play a vital role in the natural convection flow. The heat exchangers, steel manufacturing and other cooling phenomena are the prime areas where the convective heat energy transfer flow plays an important and basic role. The transfer of heat energy above a vertical and stretching surface during the magnetized flow is examined by *Nazar et al.* (2008) and noticed that the increasing magnetic field strength results in the reduction of the heat energy loss and coefficient of local skin friction.

II. MATHEMATICAL FORMULATION

We consider the thermal effect on heat and mass transfer of MHD viscoelastic fluid flow of an electrically conducting, steady and incompressible fluid flow past a plain sheet under the action of thermal and solutal buoyancy forces. A uniform transverse variable magnetic field B(x) is applied perpendicular to the direction of flow with chemical reaction taking place in the fluid flow. The transverse applied magnetic field and induced magnetic, are assumed to be very small, so that the induced magnetic field is negligible. The flow is assumed to be in the x-direction with y-axis normal to it. The flow of an incompressible and non-Newtonian fluid near an impermeable plain sheet stretching with velocity $U_w(x)$, temperature distribution $T_w(x)$, γ_0, is the non-newtonian viscoelastic parameter, g is the acceleration due to gravity, $\boldsymbol{\lambda}$ is the chemical reaction parameter and concentration distribution $C_w(x)$ moving through a quiescent ambient fluid of constant temperature T_1 and concentration C_1 were considered. The presence of thermal diffusion (Soret) and diffusion-thermo (Dufour) effects were included. The plate is maintained at the temperature and species concentration T_w, C_w and free stream temperature and species concentrationT_1, C_1 respectively. The geometry of the model and equations governing the cross-diffusion effects of heat and mass transfer of steady MHD viscoelastic fluid flow in plain porous media are detailed. In this study we consider an steady 2-D incompressible fluid which is a Newtonian flow in plain stretching sheet. The x-axis is taken in the upward direction of the plate and y-axis is taken perpendicular to the plate.

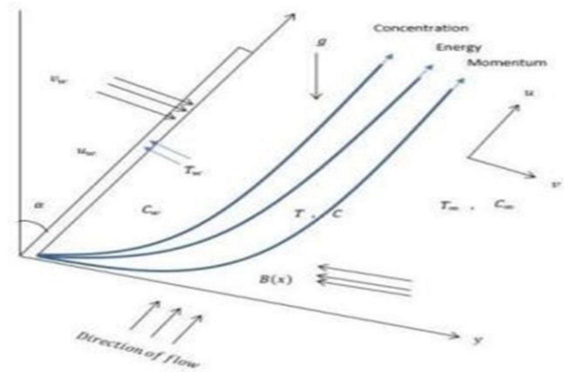

Figure 1.1: Geometry representation of the study (Amoo and Idowu, 2018, Mfebe, Amoo, Anyanwu, 2025)

$$\frac{\partial u}{\partial x} + \frac{\partial v}{\partial y} = 0 \tag{1}$$

Momentum equation

$$\frac{\partial u}{\partial t} + u\frac{\partial u}{\partial x} + v\frac{\partial u}{\partial y} = -\left(\frac{1}{\rho}\sigma B^2(x) + \frac{\nu}{K}\right)u + \nu\frac{\partial^2 u}{\partial y^2} - \gamma_0\left\{\frac{\partial^3 u}{\partial x\,\partial y^2} + \nu\frac{\partial^3 u}{\partial y^3} + \frac{\partial u}{\partial x}\frac{\partial^2 u}{\partial y^2}\right\} + g\beta_T(T - T_\infty)\cos\alpha + g\beta_C(C - C_\infty)\cos\alpha \tag{2}$$

Energy equation

$$\rho C_p\left(\frac{\partial T}{\partial t} + u\frac{\partial T}{\partial x} + v\frac{\partial T}{\partial y}\right) = \kappa\frac{\partial^2 T}{\partial y^2} - \frac{\partial q_r}{\partial y} + Q_0(T - T_\infty) + \frac{D_m\partial^2 C}{C_s\partial y^2} \tag{3}$$

concentration equation

$$\frac{\partial C}{\partial t} + u\frac{\partial C}{\partial x} + v\frac{\partial C}{\partial y} = D\frac{\partial^2 C}{\partial y^2} - \gamma(C - C_\infty) + \frac{D_m\partial^2 T}{T_m\partial y^2} \tag{4}$$

The boundary condition governing the flow are;

$$u = U_0 e^{\frac{x}{l}},\ v = -V e^{\frac{x}{l}},\ T = T_w + T_0 e^{\frac{x}{2l}},\ C = C_w + C_0 e^{\frac{x}{2l}},\ at\ y = 0$$

$$u \to 0, T \longrightarrow T_\infty, C \to C_\infty,\ y \to \infty, y \to \infty, at\ t > 0 \tag{5}$$

Where the unsteady parameter is a function of space (x, y) and time, t. By using Rossland approximation according to (Ibrahim and Suneetha, 2015, Amoo and Idowu, 2018) we have;

$$q_r = -\frac{4\sigma_0}{3\delta}\frac{\partial T^4}{\partial y} \tag{6}$$

Considering temperature differences of the flow are small such that T^4 may be expressed as a linear function of temperature, using Taylor series to expand T^4 about the free stream T_∞ and neglecting higher order terms, this gives the approximation.

$$T^4 \cong 4T_\infty^3 T - 3T_\infty^4 \quad (7)$$

Follow from (6) and (7), that equation (8) becomes

$$\left(\frac{\partial T}{\partial t} + u\frac{\partial T}{\partial x} + v\frac{\partial T}{\partial y}\right) = \left(\frac{k}{\rho C_p} + \frac{16\sigma 0 T_\infty^3}{3\delta\rho C_p}\right)\frac{\partial^2 T}{\partial y^2} + \frac{Q0}{\rho C_p}(T - T\infty) + \frac{Dm\partial^2 C}{\rho C P C s \partial y^2} \quad (8)$$

The magnetic field $B(x)$ is assumed to be in the form

$$B(x) = B_0^2 e^{\frac{x}{2l}} \quad (9)$$

Where B_0 is a constant magnetic field. We now introduce the stream function $\boldsymbol{\psi}$ (x,y) such that

$$u = \frac{\partial\psi}{\partial y} \qquad , v = -\frac{\partial\psi}{\partial x} \quad (10)$$

We substitute (10) into (1), we have the Cauchy Riemann equation, which states that given a $F(z) = u(x, y) + iv(x, y)$ be a complex function, where z = x + iy, and $u(x, y) and\ v(x, y)$ are real-valued functions. Then, F(z) is analytic at a point z_0 if and only if the following Cauchy- Riemann equations hold:

$$\frac{\partial u}{\partial x} = \frac{\partial v}{\partial y} \qquad and \quad \frac{\partial u}{\partial y} = -\frac{\partial v}{\partial x} \quad (11)$$

hence the continuity condition (1) is fully satisfied.

$$\frac{\sigma}{\partial x}\left(\frac{\sigma\psi}{\partial y}\right) - \left(\frac{\sigma}{\partial y}\right)\left(\frac{\sigma\psi}{\partial x}\right) = 0 \quad (12)$$

Considering (10) in equations (2, 3 and 8) they becomes

$$\frac{\partial^2\psi}{\partial t\partial y} + \frac{\partial\psi}{\partial y}\frac{\partial^2\psi}{\partial x\partial y} - \frac{\partial\psi}{\partial x}\frac{\partial^2\psi}{\partial y^2} = v\frac{\partial^3\psi}{\partial y^3} - \left(\frac{1}{\rho}\sigma B_0^2 e^{\frac{x}{2L}} + \frac{v}{K}\right)\frac{\partial\psi}{\partial y} - \Upsilon_0\left\{\frac{\partial\psi}{\partial y}\frac{\partial^3 u}{\partial x\partial y^2} + v\frac{\partial^3\psi}{\partial y^3} + \frac{\partial u}{\partial x}\frac{\partial^2 u}{\partial y^2}\right\} +$$
$$g\beta_r(T - T\infty)\cos\alpha + g\beta_C(C - C\infty)\cos\alpha$$

(13)

$$\left(\frac{\partial T}{\partial t} + \frac{\partial\psi}{\partial y}\frac{\partial T}{\partial x} - \frac{\partial\psi}{\partial x}\frac{\partial T}{\partial y}\right) = \left(\frac{k}{\rho C_p} + \frac{16\sigma 0 T_\infty^3}{3\delta\rho C_p}\right)\frac{\partial^2 T}{\partial y^2} + \frac{Q0}{\rho C_p}(T - T\infty) + \frac{Dm\partial^2 C}{Cs\partial y^2} \quad (14)$$

$$\frac{\partial C}{\partial t} + \frac{\partial\psi}{\partial y}\frac{\partial C}{\partial x} - \frac{\partial\psi}{\partial x}\frac{\partial C}{\partial y} = D\frac{\partial^2 C}{\partial y^2} - \gamma(C - C_\infty) + \frac{Dm\partial^2 T}{Tm\partial y^2} \quad (15)$$

In order to transform the equation (13), (14) and (15) into ordinary differential equations, we apply similarity variable (16) below according to (Sajid and Hayat, 2008; Amoo and Idowu, 2018).

$$\psi(x,y) = \sqrt{2vU_0 l}\, e^{\frac{x}{2l}} f(\eta), \eta = y\sqrt{\frac{U_0}{2vl}}\, e^{\frac{x}{2l}}, T = T\infty + T_0 e^{\frac{x}{2l}}\theta(\eta), C = C\infty + C_0 e^{\frac{x}{2l}}\phi(\eta)$$

$$\frac{\partial C}{\partial t} \neq 0\ \frac{\partial T}{\partial t} \neq 0, \frac{\partial C}{\partial t} \neq 0 \quad (16)$$

we now also define some dimensionless parameters.

$$M = \frac{2\sigma l B_0^2}{\rho U_0} e^{\frac{x}{2l}}, Pr = \frac{\mu C_p}{K}, R = \frac{4\sigma_0 T_\infty^3}{\delta K}, Sc = \frac{v}{Dm}, f_w = V_0\sqrt{\frac{2l}{vU_0}}\, e^{\left(\frac{x}{2l}\right)}, \lambda = \frac{2vl}{U_0} e^{-\left(\frac{x}{l}\right)}$$
$$Q = \frac{2lQ_0}{U_0\rho Cp} e^{-\left(\frac{x}{l}\right)}, D_u = \frac{D_m U_0}{Cs 2vl} C_0 e^{\frac{3x}{2l}}, S_r = \frac{D_m U_0}{Tm 2vl} T_0 e^{\frac{3x}{2l}}, D_a = \frac{2vl}{U_0 K} e^{-\left(\frac{x}{l}\right)}$$
$$G_r = \frac{2lg\beta_T T_0}{U_0^2} e^{\frac{3x}{2l}}, G_C = \frac{2lg\beta_C C_0}{U_0^2} e^{\frac{3x}{2l}}, U = \eta\frac{2l}{U_0} e^{-\left(\frac{x}{l}\right)}, \eta = \frac{\partial u}{\partial t}$$

(17)

III. SOLUTION OF THE PROBLEM

We follow similar steps as (Amoo and Idowu, 2018, Mfebe, Amoo, and Anyanwu, 2025). It is a step by step process where a table of function values for a range of values of x is accumulated. Summary to steps involved; (i) the shooting method replaced the given BVP by a sequence of IVPs for the same ODE with initial conditions, (ii) integrating the sequence of IVPs using embedded fourth order Runge-Kutta scheme, (iii) the integrated length varies with the parameter values and it has been suitably chosen each time such that the boundary conditions at the outer edge of boundary layer are satisfied, and (iv) Repeating this procedure till the convergence is obtained satisfying the boundary conditions.

The governing equations of heat and mass transfer of MHD fluids are essentially nonlinear ODEs. Hence, the systems of nonlinear ODEs together with the boundary conditions are solved numerically using embeded fourth order Runge-Kutta scheme with shooting techniques. The method has been proven to be adequate for boundary layer equations, seems to give accurate results and has been widely used (Ibrahim and

Makinde, 2010, Ibrahim and Suneetha, 2015, Amoo and Idowu, 2017, 2018).

$$f_{n+1} = f_n + \frac{\Delta\eta}{6}(k_1 + 2k_2 + 2k_3 + k_4) \quad (18)$$

Where

$$k_1 = \Delta\eta f(x_n, y_n)$$

$$k_2 = \Delta\eta f\left(x_n + \frac{\Delta\eta}{2}, y_n + \frac{k_1}{2}\right)$$

$$k_3 = \Delta\eta f\left(x_n + \frac{\Delta\eta}{2}, y_n + \frac{k_2}{2}\right)$$

$$k_4 = \Delta\eta f(x_n + \Delta\eta, y_n + k_3)$$

Where $\Delta\eta$=0.01 is the step size.

The patterns or arrays shows how to determine the constants or the unknown constants. from the transformed equations, (18), (19), (20), the primes indicates the derivatives with respect to η, applying RK to the problem, let defined;

$$\begin{pmatrix} x_1 \\ x_2 \\ x_3 \\ x_4 \\ x_5 \\ x_6 \\ x_7 \\ x_8 \\ x_9 \end{pmatrix} = \begin{pmatrix} \eta \\ f \\ f' \\ f'' \\ f''' \\ \theta \\ \theta' \\ \phi \\ \phi' \end{pmatrix} \quad (19)$$

$$\begin{pmatrix} x_1' \\ x_2' \\ x_3' \\ x_4' \\ x_5' \\ x_6' \\ x_7' \\ x_8' \\ x_9' \end{pmatrix} = \begin{pmatrix} 1 \\ x_3 \\ x_4 \\ x_5 \\ x_2x_4 - 2x_3^2 - Ux_4 - (M + D_a)x_3 + \lambda_1(2x_3x_5 - x_4^2) - G_r x_6 \cos(\alpha) - G_c x_8 \cos(\alpha) \\ x_7 \\ -\frac{(3Prx_2x_7 - 3Prx_2x_6 - 3PrUx_6 + 3PrQx_6 + 3PrD_u x_9)}{3 + 4R} \\ x_9 \\ -S_c(x_2x_9 - x_3x_8 - x_3x_8 - Ux_9 - \lambda x_6 + S_r x_7) \end{pmatrix}$$

Substituting, 17 and 18 into equations 13, 14 and 15 we obtain ordinary differential equations

$$f''' + ff'' - 2(f')^2 - Uf'' - (M + Da)f' - \lambda_1[2f'f''' - ff''^2 - f''^2] + G_T\theta cos\alpha + G_c\Phi \cos\alpha \quad (19)$$

$$\left(1 + \tfrac{4}{3}R\right)\theta'' + Prf\theta' - Prf'\theta - UP_r\theta + PrQ\theta + P_rD_f\phi'' = 0 \quad (20)$$

$$\Phi'' + S_cf\Phi' - S_cf'\phi - S_cU\phi' - S_c\lambda\theta + S_cS_r\theta'' = 0$$
(21)

with corresponding transformed boundary conditions takes the form;

$$f = f_w, f' = 1, \theta = 1, \Phi = 1, at\ \eta = 0$$

$$f' = 0, \theta = 0, \phi = 0, as\ \eta \to \infty \quad (22)$$

Equations (19, 20, and 21) were integrated as IVPs, the values for $f''(0), \theta'(0)$ *and* $\phi'(0)$ which are require to explain velocity, Nusselt and Sherwood numbers, were not given at the boundary. The suitable guess values for$f''(0), \theta'(0)$ *and* $\phi'(0)$ were chosen and then integrations were carried out. The obtained values were compared to the calculated values for $f''(0), \theta'(0)$ *and* $\phi'(0)$ at η = 7 with the given boundary conditions $f''(7) = 0, \theta'(7) = 0$ *and* $\phi'(7) = 0$, then adjusted the estimated values for$f''(0)$, $\theta'(0)$ *and* $\phi'(0)$, to give a better approximation for the solution. By performing series of computations to obtain values for $f''(0)$, $\theta'(0)$ *and* $\phi'(0)$, and then applied a fourth order Runge-Kutta method with shooting technique with step-size $\Delta\eta = 0.01$. The procedure was repeated until the results up to the desired degree of accuracy 10^{-6} was achieved. The effect of the computation on heat and mass transfer as well as proportional effects on the velocity, Nusselt and Sherwood number are presented and examined for different values of the independent parameters. These enabled us to use the effects of dimensionless parameters to explain cross-diffusion of heat and mass transfer of unsteady MHD flow in exponentially-stretching vertical and inclined surfaces. However, the physical quantity of practical interest are the velocity profile, the Nussett number Nu and local Sherwood number Sh defined respectively as:

$$C_f = \frac{T_w}{\rho u_w^2}, Nu = \frac{q_w x}{k(T_w - T_\infty)}, Sh = \frac{q_m x}{D_m(C_w - C_\infty)} \quad (23)$$

Where k is the thermal conductivity of the fluid, Tw, qw, $and\ qm$ are respectively given as;

$$T_w = \mu \left(\frac{\partial u}{\partial y}\right)_{y=0}, q_w = k\left(\frac{\partial T}{\partial y}\right)_{y=0}, q_m = D\left(\frac{\partial T}{\partial y}\right)_{y=0} \quad (24)$$

Therefore, the local skin friction coefficient, local Nusselt number and local Sherwood are:

$$C_f Re_x^{-\frac{1}{2}} = f''(0),\ \ Nu Re_x^{-\frac{1}{2}} = \theta'(0),\ \ Sh Re_x^{-(\frac{1}{2})} = \Phi'(0) \quad (25)$$

Where

$Re^{\frac{1}{2}} = \frac{U_w x}{v}$ is the local Reynolds number.

Therefore, Cf, Nu, $and\ Sh$ are rewritten respectively as:

$$C_f\left(\frac{U_w x}{v}\right)^{-\frac{1}{2}} = f''(0), Nu\left(\frac{U_w x}{v}\right) = \theta'(0), Sh\left(\frac{U_w x}{v}\right)^{\frac{1}{2}} = \Phi'(0) \quad (26)$$

IV. RESULT AND DISCUSSION

Our focus been the effects of; velocity profile, Nusselt and Sherwood number, which are respectively proportional to $f''(0)$, $\theta'(0)$ and $\phi'(0)$ on the dimensionless parameters using the developed mathematical model to describe the unsteady MHD flow with cross-diffusion effects of unsteady MHD viscoelastic fluid flow and analyze the combined effects of magnetic field strength, cross-diffusion coefficients, and surface inclination on heat and mass transfer. Hence solving the nonlinear model numerically, using maple 2024 embedded classical fourth order Runge-Kutta scheme alongside a shooting technique. Table 1.1, shows the comparison of the present study with previous studies, using the same values as the existing works from the literature review $\theta'(0)$ and $\phi'(0)$. By maintaining all newly introduced parameters zero. The numerical values of $\theta'(0)$ and $\phi'(0)$ at the sheet for different values of Gr, Gc, M, fw, Pr and Sc when other parameters were made zero, was done to validate our result. From which, it could be deduced that the variations of Gr. =Gc. = M = fw= 0.1 for numerical values of $\theta'(0)$ and $\phi'(0)$ at the sheet when compared with the existing literature were in close agreement. From the present study it can be concluded than the system is not affected by a change in the thermal Grashof number, but a change in the solutal Grashof and Schmidt number affects the Sherwood coefficient, ϕ'.

Table 1.1 comparing present study of Unsteady MHD fluid flow at the surface for$\theta'(0)$ and $\phi'(0)$ with previous studies of Steady MHD fluid flow for different values of Gr, Gc, M, Fw, Sc.

						Present study(2025)		Amoo & Idowu, (2018)		Lakshmi *et al*. (2012)	
Gr	Gc	M	Fw	Sc	Pr	-ϕ'(0)	-θ'(0)	-ϕ'(0)	-θ'(0	-ϕ'(0)	-θ'(0)
0.1	0.1	0.1	0.1	0.62	0.5	0.752641	0.651008	0.74019	0.80508	0.728481	0.79904
0.5	0.1	0.1	0.1	0.62	0.5	0.720677	0.621562	0.77380	0.84101	0.76248	0.83593
1.0	0.1	0.1	0.1	0.62	0.5	0.687004	0.591016	0.806773	0.87617	0.79681	0.87297
0.1	0.5	0.1	0.1	0.62	0.5	0.798879	0.694902	0.776285	0.843609	0.76491	0.83850
0.1	0.1	0.1	0.1	0.78	0.5	0.875235	0.648650	0.84118	0.803798	0.83297	0.79369

The following parameters values were adopted for computation as default values: M = 1, Gr = 1, Gc = 0.01, fw = 1, Q = 0.5, R = 0.5, Sc = 0.35, P r = 0.31, Du =0.02, Sr =0.035, λ = 0. All the computations were carried out using the values in the Table 1.2 except otherwise indicated on the graph.

Table 4.2: Effects of Dimensionless parameters on $f''(0), \theta'(0)$ *and* $\phi'(0)$.

P	Values	$-f''(0)$,	$-\theta'(0)$	$-\phi'(0)$	P	Values	$-f''(0)$,	$-\theta'(0)$	$-\phi'(0)$
M	1	1.485577	0.457614	0.461474	Da	0.001	0. 148557	0.461475	0.457614
	3	2.043786	0.426970	0.390559		1	1.485577	0.461475	0.457614
	5	2.490272	0.661794	0.342113		2.5	2.161419	0.378830	0.421999
	7	2.855581	0.39948	0.325686		3.5	2.380086	0.359401	0.413778
Gc	0.01	1.485577	0.461475	0.457614	Gr	1	1.485577	0.461475	0.457614
	3.10	1.095649	0.538770	0.493634		2	1.351436	0.493483	0.471811
	3.80	1.014232	0.550814	0.499729		3	1.223061	0.519164	0.483923
	4.50	0.934508	0.561819	0.505396		4	1.099116	0.540799	0.494596
	2	2.002124	0.658643	0.544184		8	1.627153	0.418180	0.440106
	3	2.670247	0.913547	0.650986		45	1.369774	0.489468	0.469974
	4	3.460274	1.204824	0.777549		75	1.189001	0.525360	0.486937
R	0.5	1.485577	0.461475	0.457614	Q	0.5	1.485577	0.461475	0.457614
	2	1.463977	0.481260	0.206521		1.5	1.499800	0.448756	0.642531
	5	1.473039	0.472949	0.306133		2.5	1.508733	0.441166	0.781495
	7	1.465890	0.479510	0.226980		3.5	1.515217	0.435905	0.897427
	0.62	1.485709	0.726337	0.456732		0.2	1.484951	0.462045	0.449011
	1.50	1.485863	1.138686	0.455324		2	1.478599	0.467733	0.361642
	2.00	1.486007	1.738185	0.453218		4	1.471349	0.474012	0.261733
Sr	0.035	1.485577	0.461475	0.457614	Fw	1	1.485577	0.461475	0.457614
	0.5	1.485550	0.484904	0.457776		2	1.117016	0.333129	0.388353
	1.50	1.485492	0.314614	0.458095		3	0.864227	0.258963	0.332632
	2	1.485463	0.264969	0.458260		5	0.690512	0.214169	0.287608
Pr	0.31	1.480897	0.465739	0.398923	λ	0	0. 1.485577	461475	0.457614
	0.62	1.485577	0.614750	0.457614		0.5	2.002324	0.499779	0.660771
	1.24	1.501068	0.447719	0.675482		1	1.724350	0.457614	0.555853
	2.48	1.519660	0.432417	1.005691		1.5	1.485577	0.461475	0.461474

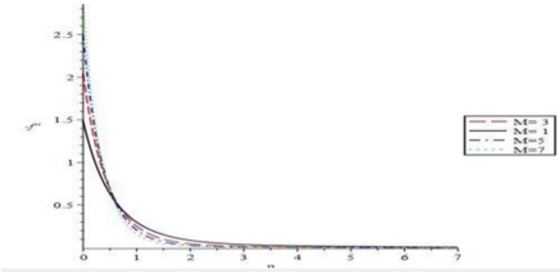

Fig 1

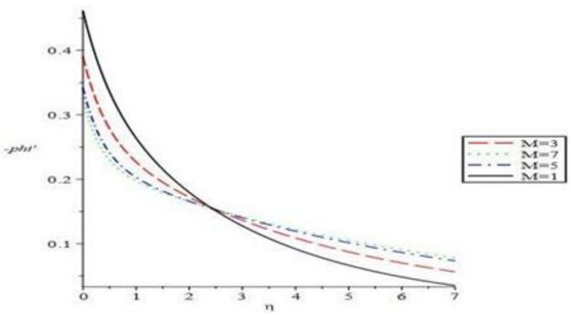

Fig 2

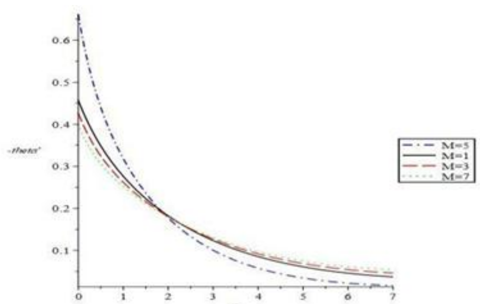

Fig 3

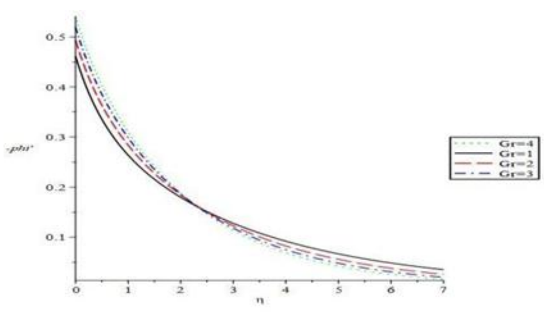

Fig 4

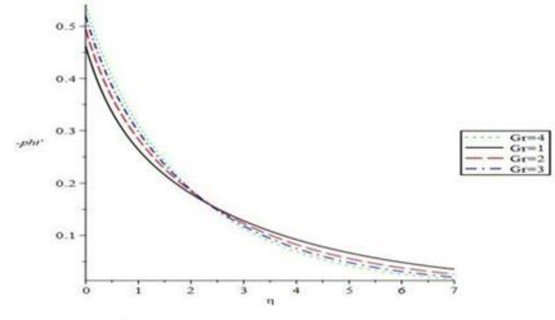

Fig 5

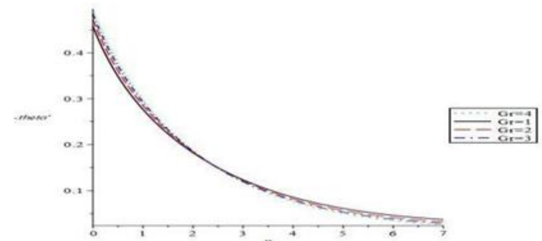

Fig 6

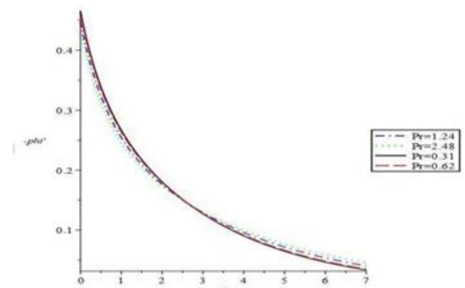

Fig 7

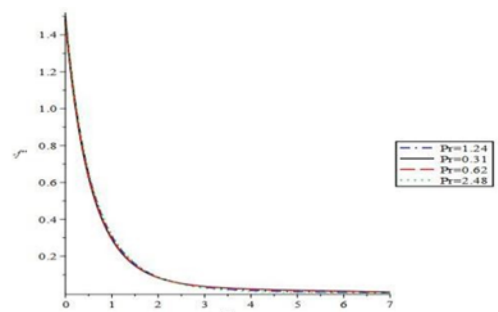

Fig 8

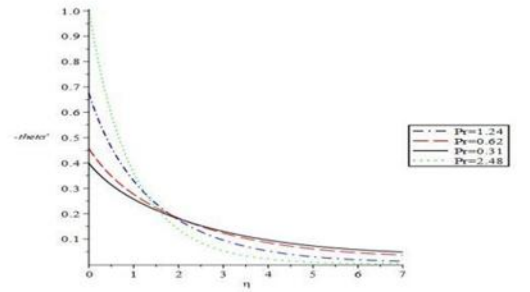

Fig 9

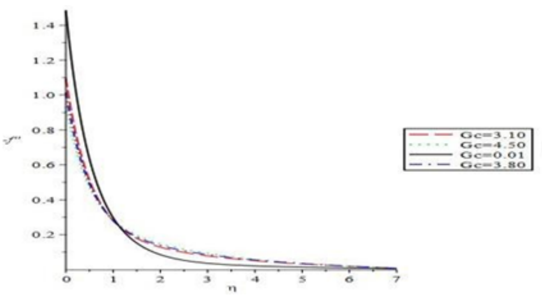

Fig 10

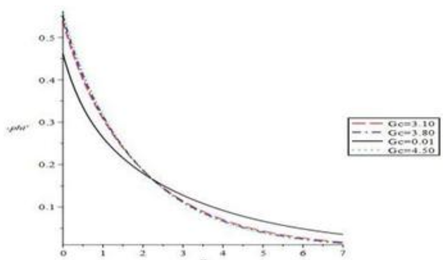

Fig 11

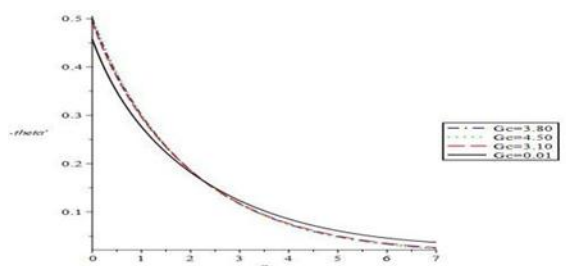

Fig 12

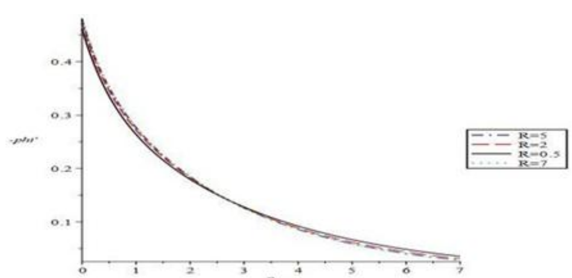

Fig 13

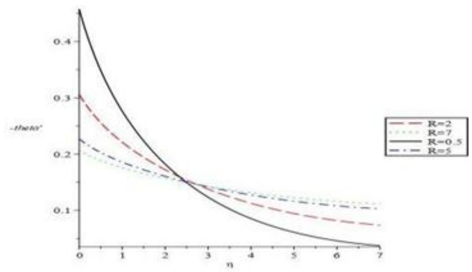

Fig 14

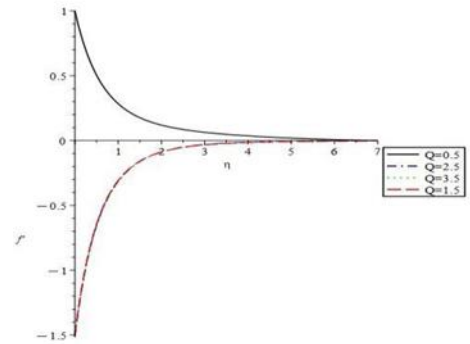

Fig 15

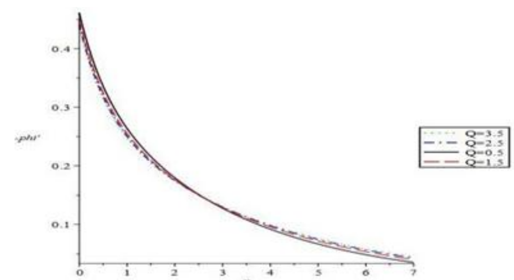

Fig 16

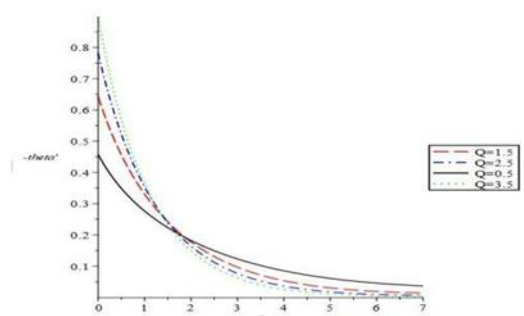

Fig 17

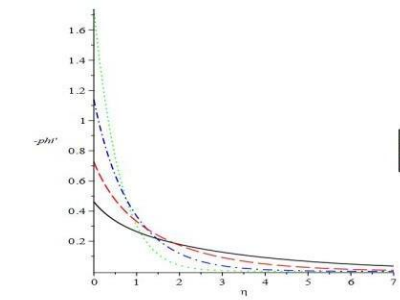

Fig 18

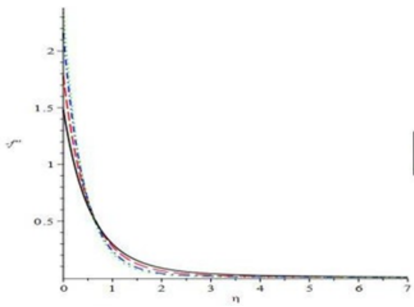

Fig 19

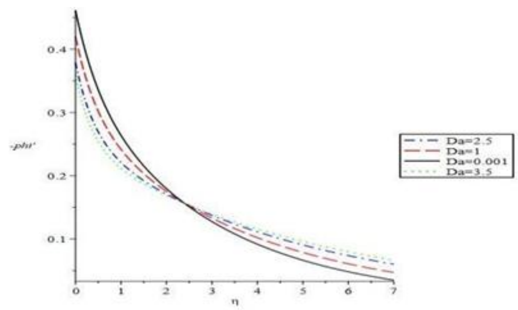

Fig 20

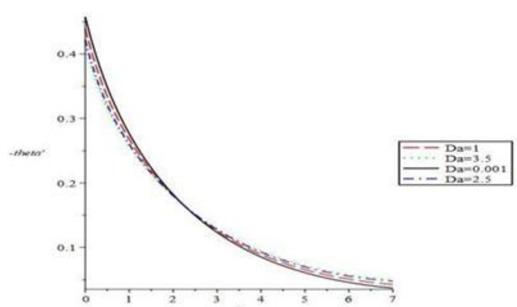

Fig 21

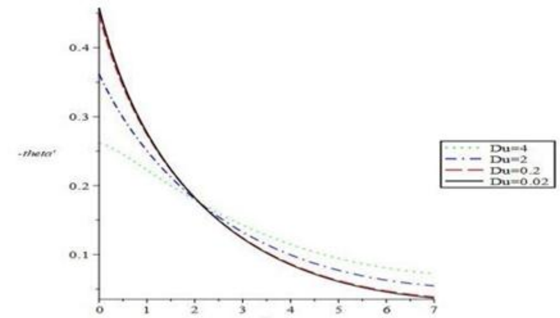

Fig 21

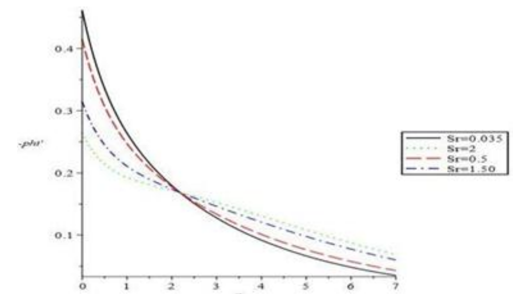

Fig 22

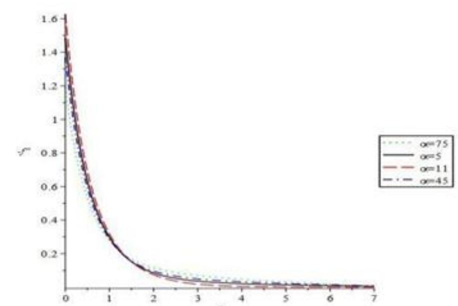

Fig 23

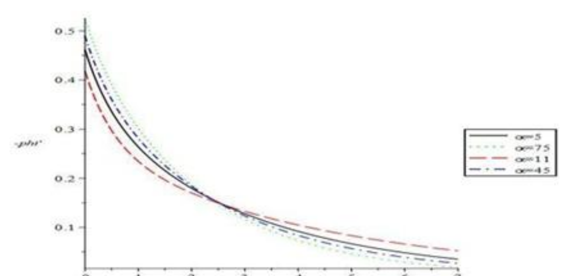

Fig 24

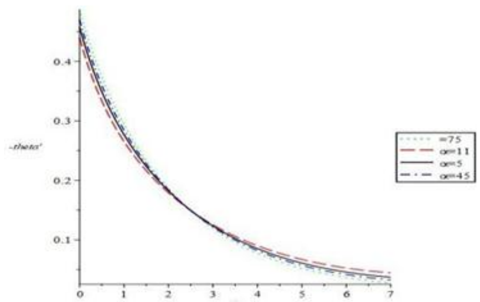

Fig 25

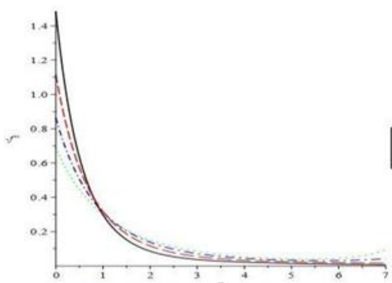

Fig 26

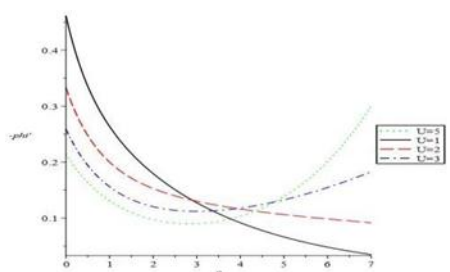

Fig 27

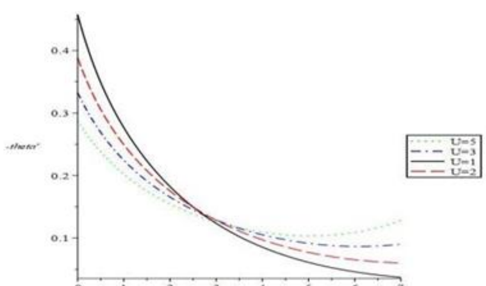

Fig 28

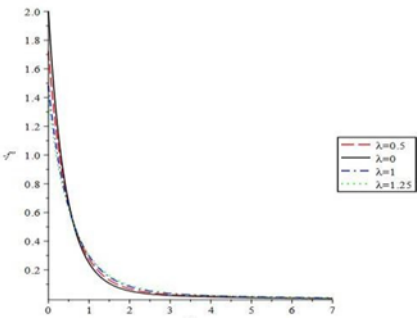

Fig 29

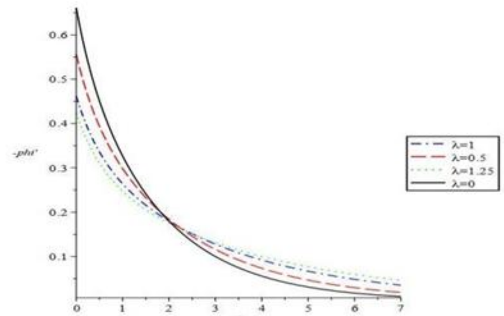

Fig 30

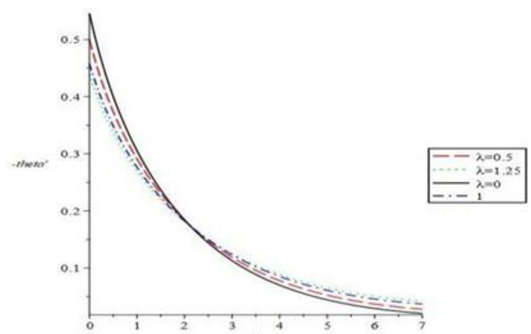

Fig 31

V. DISCUSSION

Figures 1, present the effects of magnetic field parameter on fluid flow on the velocity profile, showing that an increase in the value of M leads to an increase in the velocity distribution of the generated energy. Figure 2, also shows that an in in M lead to an increase in the local Nusselt number (temperature difference), that is the ratio of convective to conductive heat transfer at the surface increases. Figure 3, represent the effects of increased value of M on the local Sherwood number (concentration) that is the ratio of convective to mass diffusive transfer at the surface, which decreases with an increase in M. In this case, temperature and concentration at the boundary layer get thinner as magnetic field increased. Figures 4, shows that an increase in Grashof parameter (Gr) decreases the velocity profile while Figure 5, shows an increase in the ratio of convective to conductive heat transfer at the surface with increase Gr and Figure 6, also shows an increase ratio of convective to mass diffusive transfer with increase in Gr. The implication of this result suggested that slow rate of heat and free convective mass transfer was noticed. In this case, Gr slowed down the exponential temperature and concentration. In Figures 7 to 9, the analysis of Pr were presented. Figure 7 presented the effect of varied Pr on velocity profile. An increase in Pr led to increase in velocity profile. It was discovered that dimensionless velocity or exponential velocity increased near the surface. Figure 8 exhibited similar trends but with a decrease in Nusselt number. The results shown in Figures 7 and 8 indicated that Pr increased the thickness of thermal boundary layer as a result heat was unable to diffuse out of the system, hence temperature profile increased. Figure 9 explained that increased in Pr. increased the Sherwood number. The outcome of this indicated increase in diffusivity. In Figures 10, 11 and 12, exhibit the effects of Gc on the exponential velocity, temperature and concentration respectively. The effect of solutal Grashof number on velocity distribution was illustrated in Figure 10. It was noticed that increase in Gc led to decrease in exponential velocity. The values of temperature and concentration increased with varied solutal Grashof number. These analyses are true of the Figures 10, 11 and 12 due to the fact that Gc usually increase when one talks about free or natural convection thereby increasing the velocity boundary layer flow. Figure, 13 and 15 presented the effects of Fw on the velocity, temperature and concentration profiles respectively. It was discovered that increase in Fw parameter led to proportional decrease in rate of fluid flow, temperature or heat transfer as well as concentration profile or mass transfer. This parameter has more influence on velocity parameter because it is the parameter that explains the concept of porosity or permeability. The negative values explain the concept of suction while positive values of the parameter reveal the concept of injection. It was observed that suction decreased the exponential velocity, thereby indicating that suction stabilized the boundary layer development. Injection increases the velocity at the boundary layer thereby indicating that injection supports the flow to penetrate more into fluid. In Figure 14, it was discovered that temperature decreased as injection decreased, this suggests that injection does not induce cooling hence, fluid transfers to the surface. On the other hand, temperature decreases as suction increases, this means that suction leads to faster cooling of the plates. Figure 15 represents the fact that concentration decreases as the suction increases and increases as the injection increases due to respective thinner and thickness in mass boundary layer. Figures 16 to 18 indicate the effects of radiation on the velocity profile, Nusselt number and Sherwood numbers, respectively. It was discovered that increase in radiation parameter, manifest decrease in velocity and concentration profiles. It was obvious that velocity and concentration profiles decreased with increase in radiation parameter, but increase in temperature profile. The effects of these were as a result of thickness in the momentum and specie boundary layers. The increase in thermal temperature was as are result of thickness in thermal boundary layer. Figures 19, 20 and 21, is the varied values of Q (independent- heat source parameter), represents the behaviour of velocity profile coefficient, Nusselt and Sherwood number. The dimensionless explaining velocity, temperature and concentration were plotted against increased values of Q. In Figure 19 an increase in Q parameter increased fluid flow velocity. In Figure 20 it could be observed that increase in Q parameter led to corresponding change in boundary layer flow. The effect was as a result of heat source or heat sink in the boundary layer on temperature distribution. It was found that variation of Q heat source generates energy which caused the temperature of fluid to increase/decrease. The presence of heat sink in boundary absorbs energy which influenced the temperature of the fluid to increase/decrease, and as it was noticed from the figure the temperature decreased with increase in heat source/sink where $Q > 0$, while it decreased with heat sink $Q < 0$ increasing. In this case heat source/sink were experienced. In Figure 21, it was observed that increase in Q parameter led to corresponding increase in concentration. Figure 22 explained the effects of Sc on concentration, which shows that an increase in Sc led to decrease in concentration profile. Schmidt number can be defined as the ratio of momentum to the mass diffusivity. The Sc quantifies the relative effectiveness of momentum and mass transport by diffusion in the hydrodynamic or velocity and concentration boundary layers. Figure 23 explains the effects of dufour on energy, and showed increase in exponential temperature, led to increase in theNusselt number. Figures 24 explained the effects of varied Soret parameter on the exponential concentration profiles. It was discovered that increase in Sr. led to decrease in velocity, temperature but an increase in the specie or concentration distribution. This means that Sr. cannot be neglected in explaining fluid flow, heat and mass transfer phenomena. The present results compared favourably with existing literatures, similarities/contrasts were noticed with minimal errors. The reasons for the minimal errors might be due to the method or technique used in solving the problems as well as the parameters we added to the new models solved. Figure 25 to 27 present the effects of exponential velocity, temperature and specie when Darcy porosity was varied. It was discovered that increase in Da led to increase in fluid velocity but decrease in temperature and concentration profiles. There were distinct changes observed in momentum and thermal boundary layers while minute changes occurred in concentration boundary layer when Darcy porosity parameters were varied. This result probably follow the convectional flow where both shear layer, thermal and boundary layer have similar characteristics but in cases where heat transfer is influenced by conduction or radiation. The boundary layer for the velocity, temperature profile and concentration exhibited varied behavior. Figures 28 to 29 displayed the behaviour of λ and its effects on, temperature and concentration, respectively. As the λ parameter varies increasingly, the skin friction coefficient and Nusselt increased but decreased Sherwood numbers. The clear implication of the plots showed decrease in velocity, temperature and concentration profiles.

CONCLUSION

The cross-diffusion analysis effects on heat and mass transfer of unsteady magnetohydrodynamics viscoelastic fluid flow in exponentially-stretching vertical and inclined porous surfaces involving free convective flow, with thermal radiation, and the behavior of the parameters in analyzing the nonlinear PDEs using similarity transformation to arrive at a set of ordinary differential equations were obtained from the governing equations. The resulting equations were solved numerically using Maple 2024. the results show that increase in Gr, Gc, Q, R and U increase flow boundary layer while increase in M, Sc, Pr, Da, fw decrease the flow boundary layer. Also, M, Q, Sc, Da and R increase thermal boundary layer, while increase Gr, Gc, P r and fw decrease thermal boundary layer. It can also be seen that increase in M, P r, Da increase the concentration boundary layer, while increase Gr, Gc, Q, fw, R decrease the concentration boundary layer. The study concluded that solutal Grashof, thermal Grashof, magnetic parameter, radiation parameter, Dufour and Soret numbers had significant effects on unsteady MHD viscoelastic fluid flow in exponentially-stretching porous surfaces.

REFERENCES

[1] Amoo, S.A. and Idowu, A.S., (2018). Cross Diffusion effects on heat and mass transfer of magnetohydrodynamics flow in porous media over exponentially stretching surfaces. In FUW trends in science and Technology, 3 (2A), 450-460.

[2] Crane, L.J. (1970), Flow past a stretching plate. *Z. Angew. Math. Phys. ZAMP*, *21*, 645– 647.

[3] Eid, M.R-.; Mahny, K.L. (2018), Flow and heat transfer in a porous medium saturated with a Sisko nanofluid over a nonlinearly stretching sheet with heat generation/absorption. *Heat Transf. Asian Res. 47*, 54–71.

[4] Hayat, T. and Sajid, M. (2008). Analytic solution for axi-symmetric flow and heattransfer of a second grade fluid past a stretching sheet. Int. J. Heat Mass Transfer, 50, 75-84.

[5] Ibrahim SY and Makinde OD 2010. Chemically reacting MHD boundary layer flow of heat and mass transfer over a moving plate with suction. Scientific Research and Essays, 5(9), 2875-2882.

[6] Ibrahim, S. M. and Suneetha, K. (2015). Effect of heat generation and thermal radiation on MHD flow near a stagnation point on a linear stretching sheet in porous medium and presence of variable thermal conductivity and mass transfer. Journal of Comp. and Appl. Res. Mech. Engr. 4(2): 133-144.

[7] Ibrahim, S. M. and Suneetha, K. (2015). Effect of heat generation and thermal radiation on MHD flow near a stagnation point on a linear stretching sheet in porous medium and presence of variable thermal conductivity and mass transfer. Journal of Comp. and Appl. Res. Mech. Engr. 4(2): 133-144.

[8] Ishak, A.; Nazar, R.; Pop, I., (2008), Hydromagnetic flow and heat transfer adjacent to a stretching vertical sheet. *Heat Mass Transf. 44*, 921

[9] Mfebe, J. F., Amoo, S. A. and Anyanwu, E. O., (2025), Analysis of cross-diffusion effects on heat and mass transfer of unsteady magnetohydrodynamics viscoelastic fluid flow in exponentially-stretching vertical and inclined porous surfaces. A dissertation report in the department of mathematics, FUW, wukari, Nigeria.

[10] Moradikazerouni, A.; Afrand, M.; Alsarraf, J.; Mahian, O.; Wongwises, S.; Tran, M.D. (2019), Comparison of the effect of five different entrance channel shapes of a micro- channel heat sink in forced convection with application to cooling a supercomputer circuit board. *Appl. Therm. Eng. 150*, 1078–1089.

[11] Moradikazerouni, A.; Afrand, M.; Alsarraf, J.; Wongwises, S.; Asadi, A.; Nguyen, T.K. (2019), Investigation of a computer CPU heat sink under laminar forced convection using a structural stability method. *Int. J. Heat Mass Transf*, *134*, 1218–1226.

[12] Vajravelu, K, (2001), Viscous flow over a nonlinearly stretching sheet. *Appl. Math. Comput. 124*, 281–288.